

3-D Scene Data Recovery Using Omnidirectional Multibaseline Stereo

SING BING KANG

*Digital Equipment Corporation, Cambridge Research Lab, One Kendall Square, Bldg. 700,
Cambridge, MA 02139*

sbk@crl.dec.com

RICHARD SZELISKI

Microsoft Corporation, One Microsoft Way, Redmond, WA 98052-6399

szeliski@microsoft.com

Received August 9, 1996; Accepted October 14, 1996

Abstract. A traditional approach to extracting geometric information from a large scene is to compute multiple 3-D depth maps from stereo pairs or direct range finders, and then to merge the 3-D data. However, the resulting merged depth maps may be subject to merging errors if the relative poses between depth maps are not known exactly. In addition, the 3-D data may also have to be resampled before merging, which adds additional complexity and potential sources of errors.

This paper provides a means of directly extracting 3-D data covering a very wide field of view, thus by-passing the need for numerous depth map merging. In our work, cylindrical images are first composited from sequences of images taken while the camera is rotated 360° about a vertical axis. By taking such image panoramas at different camera locations, we can recover 3-D data of the scene using a set of simple techniques: feature tracking, an 8-point structure from motion algorithm, and multibaseline stereo. We also investigate the effect of median filtering on the recovered 3-D point distributions, and show the results of our approach applied to both synthetic and real scenes.

Keywords: omnidirectional stereo, multibaseline stereo, panoramic structure from motion, 8-point algorithm, scene modeling, 3-D median filtering

1. Introduction

A traditional approach to extracting geometric information from a large scene is to compute multiple (possibly numerous) 3-D depth maps from stereo pairs, and then to merge the 3-D data (Ferrie and Levine, 1987; Higuchi et al., 1993; Parvin and Medioni, 1992; Shum et al., 1994). This is not only computationally intensive, but the resulting merged depth maps may be subject to merging errors, especially if the relative poses between depth maps are not known exactly. The 3-D data may also have to be resampled before merging, which adds additional complexity and potential sources of errors. 3-D data registration and merging are very

much simplified if the motion of the stereo pair is known. One simple instance of this is fixing the location of the center of the reference camera of a stereo pair and constraining the motion of the stereo pair to rotation about the vertical axis. However, unless a motorized rotary table is used to control the amount of rotation, the rotation between successive stereo views still has to be estimated. There is still the same (but much more constrained) problem of registration and 3-D resampling, albeit with only one rotational degree of freedom.

This paper provides a means of directly extracting 3-D data covering a very wide field of view, thus by-passing the need for numerous depth map merging.

In our work, cylindrical images are first composited from sequences of images taken while the camera is rotated 360° about a vertical axis. By taking such image panoramas at different camera locations, we can recover 3-D data from the scene using a set of simple techniques: feature tracking, 8-point direct and iterative structure from motion algorithms, and multibase-line stereo.

There are several advantages to this approach. First, the cylindrical image mosaics can be built quite accurately, since the camera motion is very restricted. Second, the relative pose of the various camera locations can be determined with much greater accuracy than with regular structure from motion applied to images with narrower fields of view. Third, there is no need to build or purchase a specialized stereo camera whose calibration may be sensitive to drift over time—any conventional video camera on a tripod will suffice. Our approach can be used to construct models of building interiors, both for virtual reality applications (games, home sales, architectural remodeling), and for robotics applications (navigation).

In this paper, we describe our approach to generate 3-D data corresponding to a very wide field of view (specifically 360°), and show results of our approach on both synthetic and real scenes. We first review relevant work in Section 2 before delineating our basic approach in Section 3. The method to extract wide-angle images (i.e., *panoramic images*) is described in Section 4. Section 5 reviews the 8-point algorithm and shows how it can be applied to cylindrical panoramic images. Section 6 describes two methods for extracting 3-D point data: the first relies on unconstrained tracking and uses an 8-point structure from motion algorithm, while the second constrains the search for feature correspondences to epipolar lines (traditional stereo). We briefly outline our approach to modeling the data in Section 7—details of this are given elsewhere (Kang et al., 1995). Finally, we show results of our approach in Section 8 and close with a discussion and conclusions.

2. Relevant Work

There is a significant body of work on range image recovery using stereo; good surveys can be found in (Barnard and Fischler, 1982; Dhond and Aggarwal, 1989). Most work on stereo uses images with limited fields of view. One of the earliest work to use panoramic images is the omnidirectional stereo system

of Ishiguro et al. (1992), which uses two panoramic views. Each panoramic view is created by one of the two vertical slits of a camera image sweeping around 360°; the cameras (which are displaced in front of the rotation center) are rotated by very small angles, typically about 0.4°. One of the disadvantages of this method is the slow data acquisition, which takes about 10 minutes. The camera angular increments must be approximately $1/f$ radians, and are assumed to be known *a priori*.

Murray (1995) generalizes Ishiguro et al.'s approach by using all the vertical slits of the image (except in the paper, he uses a single image raster). This would be equivalent to structure from known motion or motion stereo. The advantage is more efficient data acquisition, done at lower angular resolution. The analysis involved in this work is similar to Bolles et al.'s (1987) spatio-temporal epipolar analysis, except that the temporal dimension is replaced by that of angular displacement.

Another related work is that of plenoptic modeling (McMillan and Bishop, 1995). The idea is to composite rotated camera views into panoramas, and based on two cylindrical panoramas, project disparity values between these locations to a given viewing position. While a disparity value is estimated for each pixel in each cylindrical panorama, no explicit 3-D model is ever constructed.

Our approach is similar to that of (McMillan and Bishop, 1995) in that we composite rotated camera views to panoramas as well. However, we go a step further by reconstructing 3-D feature points and modeling the scene based upon the recovered points. We use multiple panoramas for more accurate 3-D reconstruction.

3. Overview of Approach

Our ultimate goal is to generate a photorealistic model to be used in a variety of scenarios. We are interested in providing a simple means of generating such models. We also wish to minimize the use of CAD packages as a means of 3-D model generation, since such an effort is labor-intensive (Taylor et al., 1996). In addition, we would like to generate our 3-D scene models using off-the-shelf equipment. In our case, we use a workstation with framegrabber (real-time image digitizer) and a standard 8-mm camcorder.

Our approach is straightforward: at each camera location in the scene, we capture sequences of images

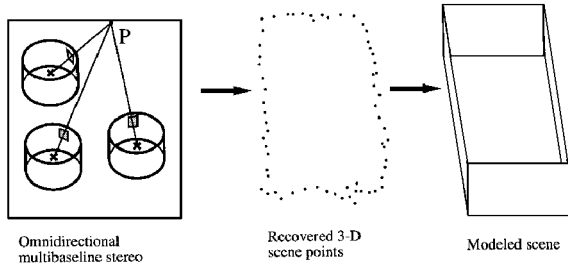


Figure 1. Generating scene model from multiple 360° panoramic views.

while rotating the camera about the vertical axis passing through the camera optical center. We composite each set of images to produce panoramas at each camera location. We use stereo to extract 3-D data of the scene. Finally, we model the scene using these 3-D data input and render it with textures extracted from the input 2-D images. Our approach is summarized in Fig. 1.

Using panoramic images, we can directly extract 3-D data covering a very wide field of view, thus by-passing the need for numerous depth map merging. Multiple depth map merging is not only computationally intensive, but the resulting merged depth maps may be subject to merging errors, especially if the relative poses between depth maps are not known exactly. The 3-D data may also have to be resampled before merging, which adds additional complexity and potential sources of errors.

Using multiple camera locations in stereo analysis significantly reduces the number of ambiguous matches and also has the effect of reducing errors by averaging (Okutomi and Kanade, 1993; Kang et al., 1995). This is especially important for images with very wide fields of view, because depth recovery is unreliable near the epipoles¹, where the looming effect takes place, resulting in very poor depth cues.

4. Extraction of Panoramic Images

A panoramic image is created by compositing a series of rotated camera images, as shown in Fig. 2. In order to create this panoramic image, we first have to ensure that the camera is rotating about an axis passing through its optical center, i.e., we must eliminate motion parallax when panning the camera around. To achieve this, we manually adjust the position of camera relative to an X-Y precision stage (mounted on the tripod) such that the motion parallax effect disappears when the camera

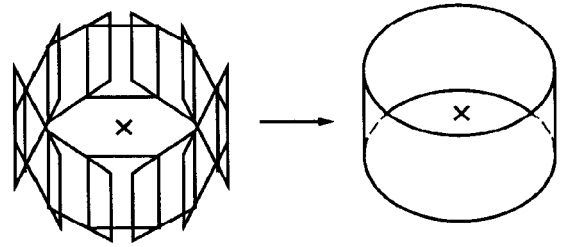


Figure 2. Compositing multiple rotated camera views into a panorama. The 'x' marks indicate the locations of the camera optical and rotation center.

is rotated back and forth about the vertical axis (Stein, 1995).

Prior to image capture of the scene, we calibrate the camera to compute its intrinsic camera parameters (specifically its focal length f , aspect ratio r , and radial distortion coefficient κ). The camera is calibrated by taking multiple snapshots of a planar dot pattern grid with known depth separation between successive snapshots. We use an iterative least-squares algorithm (Levenberg-Marquardt) to estimate camera intrinsic and extrinsic parameters (except for κ) (Szeliski and Kang, 1994). κ is determined using 1-D search (Brent's parabolic interpolation in 1-D (Press et al., 1992)), with the least-squares algorithm as the black box.

The steps involved in extracting a panoramic scene are as follow:

- At each camera location, capture a sequence while panning camera around 360°.
- Using the intrinsic camera parameters, correct the image sequence for r , the aspect ratio, and κ , the radial distortion coefficient.
- Convert the (r, κ) -corrected 2-D flat image sequence to cylindrical coordinates, with the focal length f as its cross-sectional radius. An example of a sequence of corrected images (of an office) is shown in Fig. 3.
- Composite the images (with only x -directional DOF, which is equivalent to motion in the angular dimension of cylindrical image space) to yield the desired panorama (Szeliski, 1994). The relative displacement of one frame to the next is coarsely determined by using phase correlation (Kuglin and Hines, 1975). This technique estimates the 2-D translation between a pair of images by taking 2-D Fourier transforms of both images, computing the phase difference at each frequency, performing an inverse Fourier transform, and searching for a peak in the magnitude image. Subsequently, the image translation is refined using local image

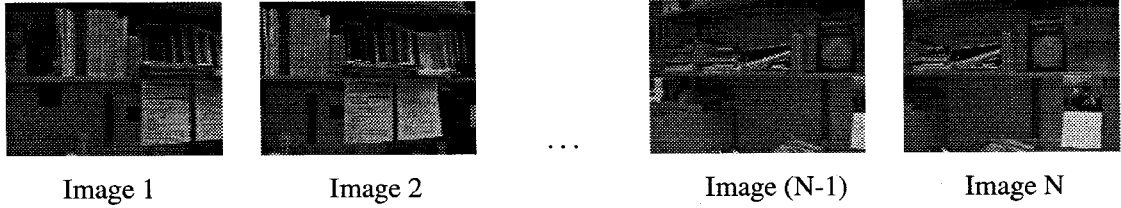


Figure 3. Example undistorted image sequence (of an office).



Figure 4. Panorama of office scene after compositing.

registration by directly comparing the overlapped regions between the two images (Szeliski, 1994, 1996).

- Correct for slight errors in the resulting length (which in theory equals $2\pi f$) by propagating residual displacement error equally across all images and recompositing. The error in length is usually within a percent of the expected length.

An example of a panoramic image created from the office scene in Fig. 3 is shown in Fig. 4.

5. Recovery of Epipolar Geometry

In order to extract 3-D data from a given set of panoramic images, we have to first know the relative positions of the camera corresponding to the panoramic images. For a calibrated camera, this is equivalent to determining the epipolar geometry between a reference panoramic image and every other panoramic image.

The epipolar geometry dictates the *epipolar constraint*, which refers to the locus of possible image projections in one image given an image point in another image. For planar image planes, the epipolar constraint is in the form of straight lines (Faugeras, 1993). For cylindrical images, epipolar curves are sinusoids (McMillan and Bishop, 1995).

We use the 8-point algorithm (Longuet-Higgins, 1981; Hartley, 1995) to extract the *essential matrix*, which yields both the relative camera placement and the epipolar geometry. This is done pairwise, namely between a reference panoramic image and another panoramic image. There are, however, four possible solutions (Longuet-Higgins, 1981; Hartley, 1995). The

solution that yields the most number of *positive* projections (i.e., projections in front of the camera) is chosen.

5.1. 8-Point Algorithm: Basics

We briefly review the 8-point algorithm here. If the camera is calibrated, i.e., its intrinsic parameters are known, then for any two corresponding image points (at two different camera placements) $(u, v, w)^T$ and $(u', v', w')^T$ in 3-D, we have

$$(u', v', w')^T E \begin{pmatrix} u \\ v \\ w \end{pmatrix} = 0 \quad (1)$$

The matrix E is called the *essential matrix*, and is of the form $E = [\mathbf{t}]_{\times} R$, where R and \mathbf{t} are the rotation matrix and translation vectors, respectively, and $[\mathbf{t}]_{\times}$ is the matrix form of the cross product with \mathbf{t} .

If the camera is not calibrated, we have a more general relation between two corresponding image points (on the image plane) $(u, v, 1)^T$ and $(u', v', 1)^T$, namely

$$(u', v', 1)^T F \begin{pmatrix} u \\ v \\ 1 \end{pmatrix} = 0 \quad (2)$$

F is called the *fundamental matrix* and is also of rank 2, $F = [\mathbf{t}]_{\times} A$, where A is an arbitrary 3×3 matrix. The fundamental matrix is the generalization of the essential matrix E , and is usually employed to establish the epipolar geometry and to recover projective depth (Faugeras, 1992; Shashua, 1994).

In our case, since we know the camera parameters, we can recover E . Let \mathbf{e} be the vector comprising e_{ij} ,

where e_{ij} is the (i, j) th element of E . Then for all the point matches, we have from (1)

$$uu'e_{11} + uv'e_{21} + uw'e_{31} + vu'e_{12} + vv'e_{22} + vw'e_{32} + wu'e_{13} + wv'e_{23} + ww'e_{33} = 0, \quad (3)$$

from which we get a set of linear equations of the form

$$\mathcal{A}\mathbf{e} = 0. \quad (4)$$

If the number of input points is small, the output of algorithm is sensitive to noise. On the other hand, it turns out that *normalizing* the 3-D point location vector on the cylindrical image reduces the sensitivity of the 8-point algorithm to noise. This is similar in spirit to Hartley's application of isotropic scaling (Hartley, 1995) prior to using the 8-point algorithm (though Hartley's algorithm is for recovering the fundamental matrix and not the essential matrix). The 3-D cylindrical points are normalized according to the relation

$$\mathbf{u} = (f \sin \theta, v, f \cos \theta) \rightarrow \hat{\mathbf{u}} = \mathbf{u}/|\mathbf{u}|, \quad (5)$$

i.e., we normalize each vector so that it is a unit direction in space. The coordinate system used for the cylinder is shown in Fig. 5.

With N panoramic images, we solve for $(N - 1)$ sets of linear equations of the form (4). The k th set

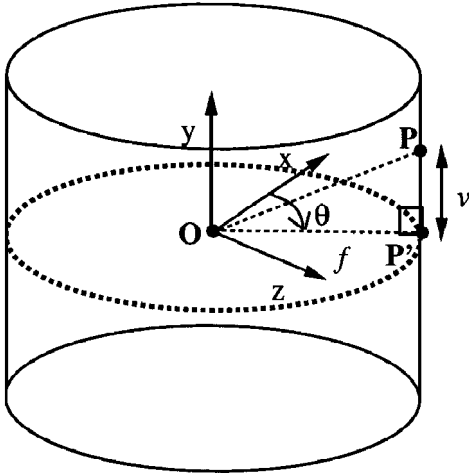


Figure 5. Cylindrical coordinate system. \mathbf{P} is any point on the cylindrical surface while \mathbf{P}' is the point projected on the x - z plane. θ is the angle subtended by the x -axis and the line segment $\mathbf{O}\text{-}\mathbf{P}$, \mathbf{O} being the center of the coordinate frame. f is the camera focal length while v is the height of point \mathbf{P} .

corresponds to the panoramic image pair 1 and $(k + 1)$. Notice that the solution for \mathbf{t} is defined only up to an unknown scale. In our work, we measure the distance between camera positions; this enables us to recover the scale. However, we can relax this assumption by carrying out the following steps:

- Fix camera distance of first pair (pair 1), to, say unit distance. Assign camera distances for all the other pairs to be the same as the first.
- Calculate the essential matrices for all the pairs of panoramic images, assuming unit camera distances.
- For each pair, compute the 3-D points.
- To estimate the relative distances between of camera positions for pair $j \neq 1$ (i.e., not the first pair), find the scale of the 3-D points corresponding to pair j that minimizes the distance error to those corresponding to pair 1. Robust statistics is used to reject outliers; specifically, only the best 50% are used. Note that outlier rejection is performed at this step of relative scale recovery only. Once the relative scales is recovered, *all* of the scaled points are used in determining the optimal merged 3-D positions.

5.2. Tracking Features for 8-Point Algorithm

The 8-point algorithm assumes that feature point correspondences are available. Feature tracking is a challenge in that purely local tracking fails because the displacement can be large (of the order of about 100 pixels, in the direction of camera motion). To mitigate this problem, we use spline-based tracking, which attempts to globally minimize the image intensity differences. This yields estimates of optic flow, which in turn is used by a local tracker to refine the amount of feature displacement.

The optic flow between a pair of cylindrical panoramic images is first estimated using spline-based image registration between the pair (Szeliski and Coughlan, 1994; Szeliski et al., 1995). In this image registration approach, the displacement fields $u(x, y)$ and $v(x, y)$ (i.e., displacements in the x - and y -directions as functions of the pixel location) are represented as two-dimensional *splines* controlled by a smaller number of displacement estimates which lie on a coarser *spline control grid*.

Once the initial optic flow has been found, the best candidates for tracking are then chosen. The choice is based on the minimum eigenvalue of the local Hessian, which is an indication of local image texturedness.

Subsequently, using the initial optic flow as an estimate displacement field, we use the Shi-Tomasi tracker (1994) with a window of size 25 pixels \times 25 pixels to further refine the displacements of the chosen point features.

Why did we use the approach of applying the spline-based tracker before using the Shi-Tomasi tracker? This approach is used to take advantage of the complementary characteristics of these two trackers, namely:

1. The spline-based image registration technique is capable of tracking features with larger displacements. This is done through coarse-to-fine image registration; in our work, we use 6 levels of resolution. While this technique generally results in good tracks (sub-pixel accuracy) (Szeliski et al., 1995), poor tracks may result in areas in the vicinity of object occlusions/disocclusions.
2. The Shi-Tomasi tracker is a local tracker that fails at large displacements. It performs better for a small number of frames and for relatively small displacements, but deteriorates at large numbers of frames and in the presence of rotation on the image plane (Szeliski et al., 1995). We are considering a small number of frames at a time, and image warping due to local image plane rotation is not expected. The Shi-Tomasi tracker is also capable of sub-pixel accuracy.

The approach that we have undertaken for object tracking can be thought of as a “fine-to-finer” tracking approach. In addition to feature displacements, the measure of reliability of tracks is available (according to match errors and local texturedness, the latter indicated by the minimum eigenvalue of the local Hessian (Shi and Tomasi, 1994; Szeliski, 1995)). As we will see later in Section 8.1, this is used to cull possibly bad tracks and improve 3-D estimates.

Once we have extracted point feature tracks, we can then proceed to recover 3-D positions corresponding to these feature tracks. 3-D data recovery is based on the simple notion of stereo.

6. Omnidirectional Multibaseline Stereo

The idea of extracting 3-D data simultaneously from more than the theoretically sufficient number of two camera views is founded on two simple tenets: statistical robustness from redundancy and disambiguation of matches due to overconstraints (Okutomi and Kanade,

1993; Kang et al., 1995). The notion of using multiple camera views is even more critical when using panoramic images taken at the same vertical height, which results in the epipoles falling *within* the images. If only two panoramic images are used, points that are close to the epipoles will not be reliable. It is also important to note that this problem will persist if all the multiple panoramic images are taken at camera positions that are collinear. In the experiments described in Section 8, the camera positions are deliberately arranged such that all the positions are *not* collinear. In addition, all the images are taken at the same vertical height to maximize view overlap between panoramic images.

We use three related approaches to reconstruct 3-D from multiple panoramic images. 3-D data recovery is done either by (1) using just the 8-point algorithm on the tracks and directly recovering the 3-D points, or (2) proceeding with an iterative least-squares method to refine both camera pose and 3-D feature location, or (3) going a step further to impose epipolar constraints in performing a full multiframe stereo reconstruction. The first approach is termed as *unconstrained tracking and 3-D data merging* while the second approach is *iterative structure from motion*. The third approach is named *constrained depth recovery using epipolar geometry*.

6.1. Reconstruction Method 1: Unconstrained Feature Tracking and 3-D Data Merging

In this approach, we use the tracked feature points across all panoramic images and apply the 8-point algorithm. From the extracted essential matrix and camera relative poses, we can then directly estimate the 3-D positions.

The sets of 2-D image data are used to determine (pairwise) the essential matrix. The recovery of the essential matrix turns out to be reasonably stable; this is due to the large (360°) field of view. A problem with the 8-point algorithm is that optimization occurs in function space and not image space, i.e., it is not minimizing error in distance between 2-D image point and corresponding epipolar line. Deriche et al. (1994) use a robust regression method called *least-median-of-squares* to minimize distance error between expected (from the estimated fundamental matrix) and given 2-D image points. We have found that extracting the essential matrix using the 8-point algorithm is relatively stable as long as (1) the number of points is large (at least in the

hundreds), and (2) the points are well distributed over the field of view.

In this approach, we use the same set of data to recover Euclidean shape. In theory, the recovered positions are only true up to a scale. Since the distance between camera locations are known and measured, we are able to get the true scale of the recovered shape. Note, however, that this approach does not depend critically on knowing the camera distances, as indicated in Section 5.1.

Once we have recovered the camera poses, i.e., the rotation matrices and translation vectors, we use the following method for estimating the 3-D point positions \mathbf{p}_i . Let \mathbf{u}_{ik} be the i th point of image k , $\hat{\mathbf{v}}_{ik}$ be the unit vector from the optical center to the panoramic image point in 3-D space, Λ_{ik} be the corresponding line passing through both the optical center and panoramic image point in space, and \mathbf{t}_k be the camera translation associated with the k th panoramic image (note that $\mathbf{t}_1 = \mathbf{0}$). The equation of line Λ_{ik} is then $\mathbf{r}_{ik} = \lambda_{ik} \hat{\mathbf{v}}_{ik} + \mathbf{t}_k$. Thus, for each point i (that is constrained to lie on line Λ_{i1}), we minimize the error function

$$\mathcal{E}_i = \sum_{k=2}^N \|\mathbf{r}_{i1} - \mathbf{r}_{ik}\|^2 \quad (6)$$

where N is the number of panoramic images. By taking the partial derivatives of \mathcal{E}_i with respect to λ_{ij} , $j = 1, \dots, N$, equating them to zero, and solving, we get

$$\lambda_{i1} = \frac{\sum_{k=2}^N \mathbf{t}_k^T (\hat{\mathbf{v}}_{i1} - (\hat{\mathbf{v}}_{i1}^T \hat{\mathbf{v}}_{ik}) \hat{\mathbf{v}}_{ik})}{\sum_{k=2}^N (1 - (\hat{\mathbf{v}}_{i1}^T \hat{\mathbf{v}}_{ik})^2)}, \quad (7)$$

from which the reconstructed 3-D point is calculated using the relation $\mathbf{p}_{i1} = \lambda_{i1} \hat{\mathbf{v}}_{i1}$. Note that a more optimal manner of estimating the 3-D point is to minimize the expression

$$\mathcal{E}_i = \sum_{k=1}^N \|\mathbf{p}_{i1} - \mathbf{r}_{ik}\|^2 \quad (8)$$

A detailed derivation involving (8) is given in Appendix A.1. To simplify the inverse texture-mapping of the input images onto the recovered 3-D mesh of the estimated points, the projections of the estimated 3-D points have to coincide with the 2-D image locations in the reference image. This can be justified by saying that since the feature tracks originate from the reference

image, it is reasonable to assume that there is no uncertainty in feature location in the reference image (see (Azarbayejani and Pentland, 1995) for a discussion of similar ideas).

An immediate problem with the approach of feature tracking and data merging is its reliance on tracking, which makes it relatively sensitive to tracking errors. It inherits the problems associated with tracking, such as the aperture problem and sensitivity to changing amounts of object distortion at different viewpoints. However, this problem is mitigated if the number of sampled points is large. In addition, the advantage is that there is no need to specify minimum and maximum depths and resolution associated with multibaseline stereo depth search (e.g., see (Okutomi and Kanade, 1993; Kang et al., 1995)). This is because the points are extracted directly analytically once the correspondence is established.

6.2. Reconstruction Method 2: Iterative Panoramic Structure from Motion

The 8-point algorithm recovers the camera motion parameters directly from the panoramic tracks, from which the corresponding 3-D points can be computed. However, the camera motion parameters may not be optimally recovered, even though experiments by Hartley using narrow view images indicate that the motion parameters are close to optimal (Hartley, 1995). Using the output of the 8-point algorithm and the recovered 3-D data, we can apply an iterative least-squares minimization to refine both camera motion and 3-D positions *simultaneously*. This is similar to work done by Szeliski and Kang on structure from motion using multiple narrow camera views (Szeliski and Kang, 1994).

As input to our reconstruction method, we use 3-D *normalized* locations of cylindrical image points. The equation linking a 3-D normalized cylindrical image position \mathbf{u}_{ij} in frame j to its 3-D position \mathbf{p}_i , where i is the track index, is

$$\mathbf{u}_{ij} = \mathcal{P}(\mathbf{R}_j^{(k)} \mathbf{p}_i + \mathbf{t}_j^{(k)}) = \mathcal{F}(\mathbf{p}_i, \mathbf{q}_j, \mathbf{t}_j) \quad (9)$$

where $\mathcal{P}(\cdot)$ is the projection transformation; $\mathbf{R}_j^{(k)}$ and $\mathbf{t}_j^{(k)}$ are the rotation matrix and translation vector, respectively, associated with the relative pose of the j th camera. We represent each rotation by a quaternion $\mathbf{q} = [w, (q_0, q_1, q_2)]$ with a corresponding rotation

matrix

$$\mathbf{R}(\mathbf{q}) = \begin{pmatrix} 1 - 2q_1^2 - 2q_2^2 & 2q_0q_1 - 2wq_2 & 2q_0q_2 + 2wq_1 \\ 2q_0q_1 + 2wq_2 & 1 - 2q_0^2 - 2q_2^2 & 2q_1q_2 - 2wq_0 \\ 2q_0q_2 - 2wq_1 & 2q_1q_2 + 2wq_0 & 1 - 2q_0^2 - 2q_1^2 \end{pmatrix} \quad (10)$$

(alternative representations for rotations are discussed in (Ayache, 1991)).

The projection equation is given simply by

$$\begin{pmatrix} u \\ v \\ w \end{pmatrix} = \mathcal{P} \begin{pmatrix} x \\ y \\ z \end{pmatrix} \equiv \frac{1}{\sqrt{x^2 + y^2 + z^2}} \begin{pmatrix} x \\ y \\ z \end{pmatrix} \quad (11)$$

In other words, all the 3-D points are projected onto the surface of a 3-D unit sphere.

To solve for the structure and motion parameters simultaneously, we use the iterative Levenberg-Marquardt algorithm. The Levenberg-Marquardt method is a standard non-linear least squares technique (Press et al., 1992) that works well in a wide range of situations. It provides a way to vary smoothly between the inverse-Hessian method and the steepest descent method.

The merit or objective function that we minimize is

$$\mathcal{C}(\mathbf{a}) = \sum_i \sum_j c_{ij} |\mathbf{u}_{ij} - \mathcal{F}(\mathbf{a}_{ij})|^2, \quad (12)$$

where $\mathcal{F}(\cdot)$ is given in (9) and

$$\mathbf{a}_{ij} = (\mathbf{p}_i^T, \mathbf{q}_j^T, \mathbf{t}_j^T)^T \quad (13)$$

is the vector of structure and motion parameters which determine the image of point i in frame j . The weight c_{ij} in (12) describes our confidence in measurement \mathbf{u}_{ij} , and is normally set to the inverse variance σ_{ij}^{-2} . We set $c_{ij} = 1$.

The Levenberg-Marquardt algorithm first forms the approximate Hessian matrix

$$\mathbf{A} = \sum_i \sum_j c_{ij} \left(\frac{\partial \mathcal{F}(\mathbf{a}_{ij})}{\partial \mathbf{a}} \right)^T \frac{\partial \mathcal{F}(\mathbf{a}_{ij})}{\partial \mathbf{a}} \quad (14)$$

and the weighted gradient vector

$$\mathbf{b} = - \sum_i \sum_j c_{ij} \left(\frac{\partial \mathcal{F}(\mathbf{a}_{ij})}{\partial \mathbf{a}} \right)^T \mathbf{e}_{ij}, \quad (15)$$

where $\mathbf{e}_{ij} = \mathbf{u}_{ij} - \mathcal{F}(\mathbf{a}_{ij})$ is the image plane error of point i in frame j . Given a current estimate of \mathbf{a} , it computes an increment $\delta \mathbf{a}$ towards the local minimum by solving

$$(\mathbf{A} + \lambda \mathbf{I}) \delta \mathbf{a} = -\mathbf{b}, \quad (16)$$

where λ is a stabilizing factor which varies over time (Press et al., 1992). Note that the matrix \mathbf{A} is an approximation to the Hessian matrix, as the second-derivative terms are left out. As mentioned in (Press et al., 1992), inclusion of these terms can be destabilizing if the model fits badly or is contaminated by outlier points.

To compute the required derivatives for (14) and (15), we compute derivatives with respect to each of the fundamental operations (perspective projection, rotation, translation) and apply the chain rule. The equations for each of the basic derivatives are given in Appendix A.2. The derivation is exactly the same as in (Szeliski and Kang, 1994), except for the projection equation.

6.3. Reconstruction Method 3: Constrained Depth Recovery Using Epipolar Geometry

As a result of the first reconstruction method's reliance on tracking, it suffers from the aperture problem and hence limited number of reliable points. The approach of using the epipolar geometry to limit the search is designed to reduce the severity of this problem. Given the epipolar geometry, for each image point in the reference panoramic image, a constrained search is performed along the line of sight through the image point. Subsequently, the position along this line which results in minimum match error at projected image coordinates corresponding to other viewpoints is chosen. Using this approach results in a denser depth map, due to the epipolar constraint. This constraint reduces the aperture problem during search (which theoretically only occurs if the direction of ambiguity is along the epipolar line of interest). The principle is the same as that described in (Kang et al., 1995).

The principle of multibaseline stereo in the context of multiple panoramic images is shown in Fig. 6. In that figure, take panoramic image with center \mathbf{O}_1 as the reference image. Suppose we are interested in determining the depth associated with image point \mathbf{u} as shown in Fig. 6. Given minimum and maximum depths as well as the depth resolution, we then project hypothesized 3-D points onto the rest of the panoramic

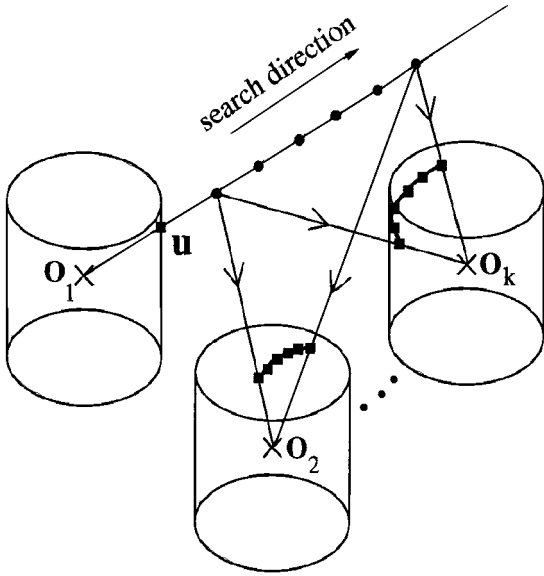


Figure 6. Principle of omnidirectional multibaseline stereo. $O_1 \dots O_k$ represent the centers of the panoramic images 1 to k , respectively, with panoramic image 1 taken to be the reference image.

images (six points in our example). For each hypothesized point in the search, we find the sum of squared intensity errors between the local windows centered at the projected image points and the local window in the reference image. The hypothesized 3-D point that results in the minimum error is then taken to be the correct location. Note that the 3-D points on a straight line are projected to image points that lie on a sinusoidal curve on the cylindrical panoramic image. The window size that we use is 25×25 . The results do not seem to change significantly with slight variation of the window size (e.g., 23×23 and 27×27). There was significant degradation in the quality of the results for small window sizes (we have tried 11×11).

While this approach mitigates the aperture problem, it suffers from a much higher computational demand. In addition, the recovered epipolar geometry is still dependent on the output quality of the 8-point algorithm (which in turn depends on the quality of tracking). The user has to also specify minimum and maximum depths as well as resolution of depth search.

An alternative to working in cylindrical coordinates is to project sections of cylinder to a tangential rectilinear image plane, rectify it, and use the rectified planes for multibaseline stereo. This mitigates the computational demand as search is restricted to horizontal scanlines in the rectified images. However, there is a major problem with this scheme: reprojecting to rectilinear

coordinates and rectifying is problematical due to the increasing distortion away from the new center of projection. This creates a problem with matching using a window of a fixed size. As a result, this scheme of reprojecting to rectilinear coordinates and rectifying is not used.

A point can be made of using the original image sequences in the projection onto composite planar images to get scan-line epipolar geometry for a speedier stereo matching process. There are the questions as to what the optimal projection directions should be and how many projections should be used. The simplest approach, as described in the previous paragraph, would be to project subsets of images to pairwise tangent planes. However, because the relative rotation within the image sequence cannot be determined *exactly*, one would still encounter the problem of constructing composite planar images that are not exactly physically correct. In addition, one would still have to use a variable window size scheme due to the varying amount of distortion across the composite planar image (e.g., comparing a local low-distortion area in the middle of one composite planar image with another that has high distortion near a side of another composite planar image). Our approach to directly use the cylindrical images is mostly out of expediency.

7. Stereo Data Segmentation and Modeling

Once the 3-D stereo data has been extracted, we can then model them with a 3-D mesh and texture-map each face with the associated part of the 2-D image panorama. We have done work to reduce the complexity of the resulting 3-D mesh by planar patch fitting and boundary simplification. Our simplification and noise reduction algorithm is based on a segmentation of the input surface mesh into surface patches using a least squares fitting of planes. Simplification is achieved by extracting, approximating, and triangulating the boundaries between surface patches. The displayed models shown in this paper are rendered using our modeling system. A more detailed description of model extraction from range data is given in (Kang et al., 1995).

8. Experimental Results

In this section, we present the results of applying our approach to recover 3-D data from multiple panoramic images. We have used both synthetic and real images to

test our approach. As mentioned earlier, in the experiments described in this section, the camera positions are deliberately arranged so that all of the positions are not collinear. In addition, all the images are taken at the same vertical height to maximize overlap between panoramic images.

8.1. Synthetic Scene

The synthetic scene is a room comprising objects such as tables, tori, cylinders, and vases. One half of the room is textured with a mandrill image while the other is textured with a regular Brodatz pattern. The synthetic objects and images are created using Rayshade, which is a program for creating ray-traced color images (Kolb, 1994). The synthetic images created are free from any radial distortion, since Rayshade is currently unable to model this camera characteristic. The omnidirectional synthetic depth map of the entire room is created by merging the depth maps associated with the multiple views taken around inside the room.

The composite panoramic view of the synthetic room from its center is shown in Fig. 7. From left to right, we can observe the vases resting on a table, vertical cylinders, a torus resting on a table, and a larger torus. The results of applying both reconstruction methods (i.e., unconstrained search with 8-point and constrained search using epipolar geometry) can be seen in Fig. 8. We get many more points using constrained search (about 3 times more), but the quality of the 3-D reconstruction appears more degraded (compare Fig. 8(b) with (d)). This is in part due to matching occurring at integral values of pixel positions, limiting its depth resolution. The dimensions of the synthetic room are 10 (length) \times 8 (width) \times 6 (height), and the specified resolution is 0.01. The quality of the recovered 3-D data appears to be enhanced by applying a 3-D median filter.

The median filter works in the following manner: For each feature point in the cylindrical panoramic image, find other feature points within a certain neighborhood radius (20 in our case). Then sort the 3-D depths associated with the neighborhood feature points,



Figure 7. Panorama of synthetic room after compositing.

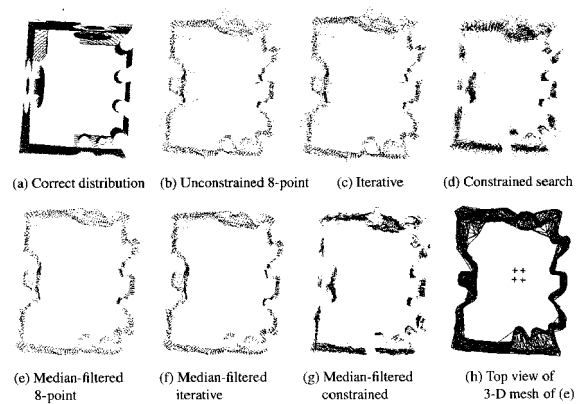


Figure 8. Comparison of 3-D points recovered of synthetic room. The four camera locations are indicated by +’s in (h).

find the median depth, and *rescale* the depth associated with the current feature point such that the new depth is the median depth. As an illustration, suppose the original 3-D feature location is $\mathbf{v}_i = d_i \hat{\mathbf{v}}_i$, where d_i is the original depth and $\hat{\mathbf{v}}_i$ is the 3-D unit vector from the camera center in the direction of the image point. If d_{med} is the median depth within its neighborhood, then the filtered 3-D feature location is given by $\mathbf{v}'_i = (d_{\text{med}}/d_i)\mathbf{v}_i = d_{\text{med}}\hat{\mathbf{v}}_i$. However, the median filter also has the effect of rounding off corners.

The mesh in Fig. 8(h) and the three views in Fig. 9 are generated by our 3-D modeling system described in (Kang et al., 1995). As can be seen from these figures, the 3-D recovered points and the subsequent model based on these points basically preserved the shape of the synthetic room. While shape distortions can be easily seen at the edges, texture-mapping tends to reduce the visual effect of incorrectly recovered shapes away from the edges.

In addition, we performed a series of experiments to examine the effect of both “bad” track removal and median filtering on the quality of recovered depth information of the synthetic room. The feature tracks are sorted in increasing order according to the error in matching². We continually remove tracks that have the worst amount of match error, recovering the 3-D point distribution at each instant.

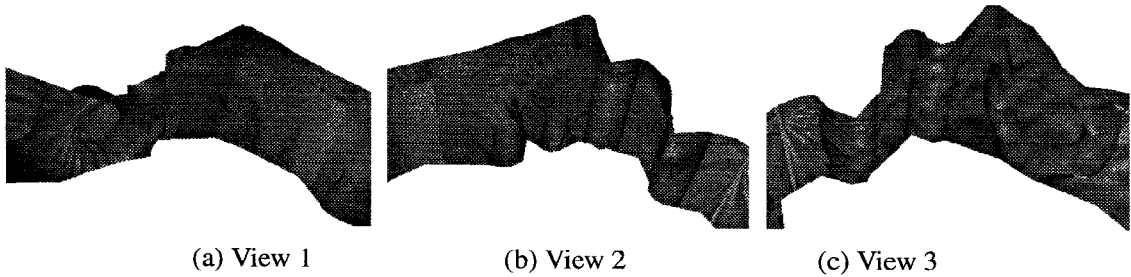


Figure 9. Three views of modeled synthetic room of Fig. 8(h). Note the distorted shape of the torus in (c) and the top parts of the cylinders in (b) and (c) that do not look circular.

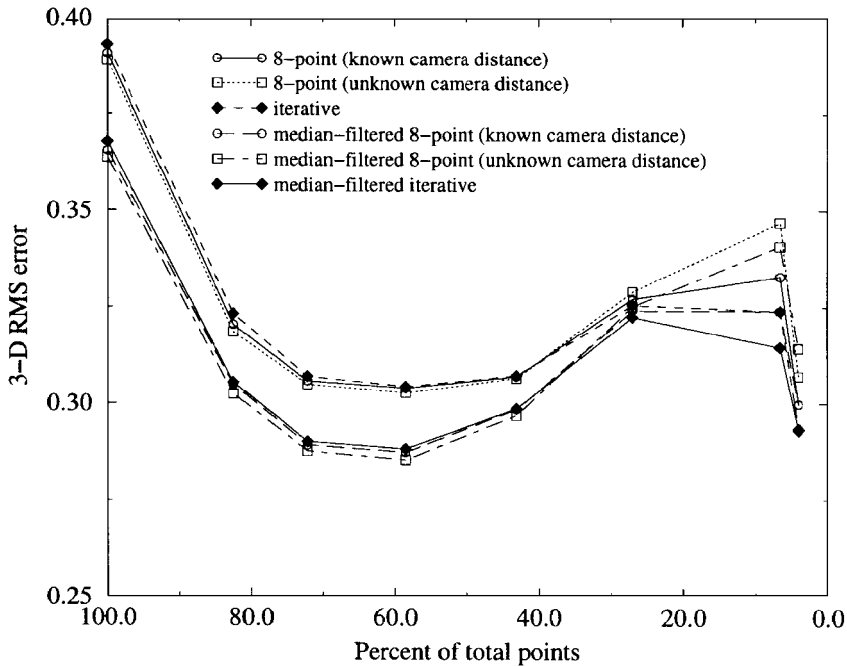


Figure 10. 3-D RMS error vs. number of points. The original number of points (corresponding to 100%) is 3057. The dimensions of the synthetic room are 10 (length) \times 8 (width) \times 6 (height). Note that by “8-point”, we mean the reconstruction method 1, with the application of the 8-point algorithm and direct 3-D position calculation. The “iterative” method is reconstruction method 2. The results of reconstruction method 3 is not represented here because the selected points (2-D location and sample size) are different.

From the graph in Fig. 10, we see an interesting result: as more tracks are taken out, retaining the better ones, the quality of 3-D point recovery improves—up to a point. The improvement in the accuracy is not surprising, since the worse tracks, which are more likely to result in worse 3-D estimates, are removed. However, as more and more tracks are removed, the gap between the amount of accuracy demanded of the tracks, given an increasingly smaller number of available tracks, and the track accuracy available, grows. This results in generally worse estimates of the epipolar geometry, and hence 3-D data. Concomitant to the

reduction of the number of points is the sensitivity of the recovery of both epipolar geometry (in the form of the essential matrix) and 3-D data. This is evidenced by the fluctuation of the curves at the lower end of the graph. Another interesting result that can be observed is that the 3-D point distribution that has been median filtered have lower errors, especially for higher numbers of recovered 3-D points.

As indicated by the graph in Fig. 10, the accuracy of the point distribution derived from just the 8-point algorithm is almost equivalent to that of using an iterative least-squares (Levenberg-Marquardt)

Table 1. Comparison of 3-D RMS error between unconstrained and constrained stereo results (n is the number of points).

| | Constrained ($n = 10040$) | 8-point ($n = 3057$) | 8-point ($n = 1788$) |
|-----------------|--------------------------------|---------------------------|---------------------------|
| Original | 0.315039 | 0.393777 | 0.302287 |
| Median-filtered | 0.266600 | 0.364889 | 0.288079 |

minimization, which is statistically optimal near the true solution. This result is in agreement with Hartley's application of the 8-point algorithm to narrow-angle images (Hartley, 1995). It is also worth noting that the accuracy of the iterative algorithm is best at smaller numbers of input points, suggesting that it is more stable given a smaller number of input data.

Table 1 lists the 3-D errors of both constrained and unconstrained (8-point only) methods for the synthetic scenes. It appears from this result that the constrained method yields better results (after median filtering) and more points (a result of reducing the aperture problem). In practice, as we shall see in the next section, problems due to misestimation of camera intrinsic parameters (specifically focal length, aspect ratio and radial distortion coefficient) causes 3-D reconstruction from real images to be worse. This is a subject of on-going research.

8.2. Real Scenes

The setup that we used to record our image sequences consists of a DEC Alpha workstation with a J300 framegrabber, and a camcorder (Sony Handycam CCD-TR81) mounted on an X-Y position stage affixed on a tripod stand. The camcorder settings are made such that its field of view is maximized (at about 43°).

To reiterate, our method of generating the panoramic images is as follows:

- Calibrate the camcorder using an iterative Levenberg-Marquardt least-squares algorithm (Szeliski and Kang, 1994).
- Adjust the X-Y position stage while panning the camera left and right to remove the effect of motion parallax; this ensures that the camera is then rotated about its optical center.
- At each camera location, record onto tape an image sequence while rotating the camera, and then digitize the image sequence using the framegrabber.

- Using the recovered camera intrinsic parameters (focal length, aspect ratio, radial distortion factor), undistort each image.
- Project each image, which is in rectilinear image coordinates, into cylindrical coordinates (whose cross-sectional radius is the camera focal length).
- Composite the frames into a panoramic image. The number of frames used to extract a panoramic image in our experiments is typically about 50.

We recorded image sequences of two scenes, namely an office scene and a lab scene. A panoramic image of the office scene is shown in Fig. 4. We extracted four panoramic images corresponding to four different locations in the office. (The spacing between these locations is about 6 inches and the locations are roughly at the corners of a square. The size of the office is about 10 feet by 15 feet.) The results of 3-D point recovery of the office scene is shown in Fig. 11, with three sample views of its model shown in Fig. 12. As can be seen from Fig. 11, the results due to the constrained search

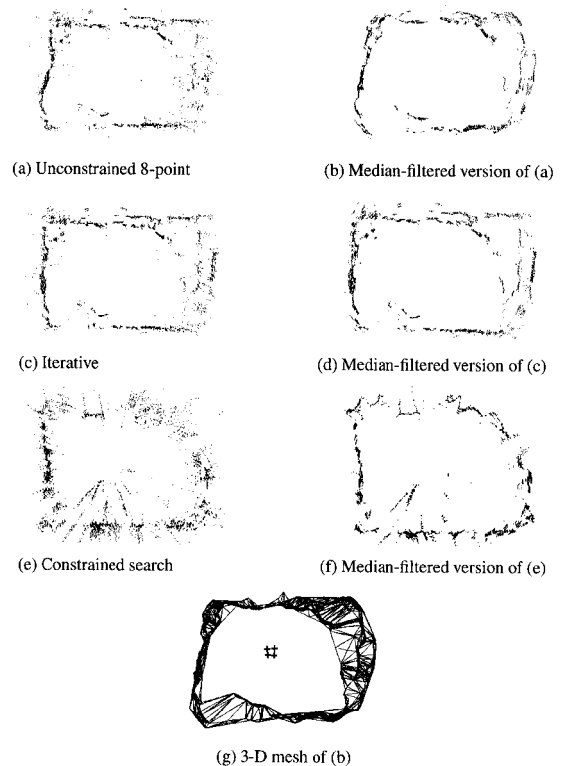


Figure 11. Extracted 3-D points and mesh of office scene. Notice that the recovered distributions shown in (c) and (d) appear more rectangular than those shown in (a) and (b). The camera locations are indicated by +'s in (g).

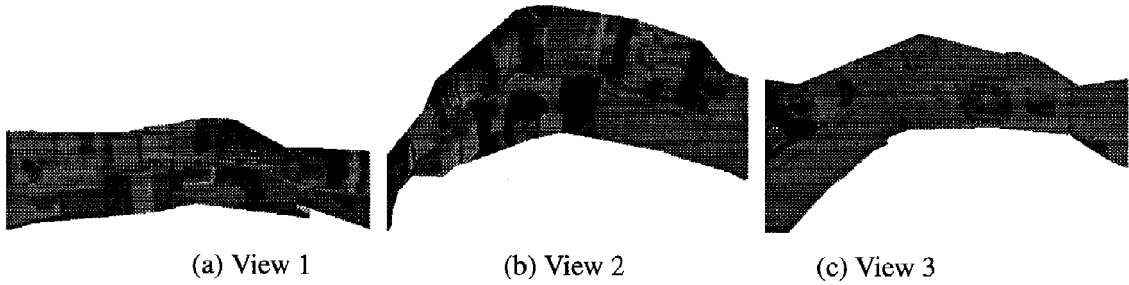


Figure 12. Three texture-mapped views of the modeled office scene of Fig. 11(g).

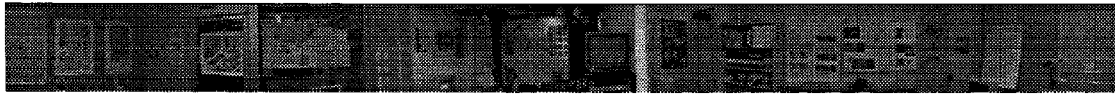


Figure 13. Panorama of laboratory after compositing.

approach looks much worse. This may be directly attributed to the inaccuracy of the extracted intrinsic camera parameters. As a consequence, the composited panoramas may actually be not exactly physically correct. In fact, as the matching (with epipolar constraint) is in progress, it has been observed that the actual correct matches are not exactly along the epipolar lines; there are slight vertical drifts, generally of the order of about one or two pixels.

Another example of a real scene is shown in Fig. 13. A total of eight panoramas at eight different locations (about 3 inches apart, ordered roughly in a zig-zag fashion) in the lab are extracted. The longest dimensions of the L-shaped lab is about 15 feet by 22.5 feet. The 3-D point distribution is shown in Fig. 14 while Fig. 15 shows three views of the recovered model of the lab. As can be seen, the shape of the lab has been reasonably well recovered; the “noise” points at the bottom of Fig. 14(a) corresponds to the positions *outside* the laboratory, since there are parts of the transparent laboratory window that are not covered. This reveals one of the weaknesses of any correlation-based algorithm (namely all stereo algorithms); they do not work well with image reflections and transparent material. Again, we observe that the points recovered using constrained search is worse.

The errors that were observed with the real scene images, especially with constrained search, are due to the following practical problems:

- The auto-iris feature of the camcorder used cannot be deactivated (even though the focal length was kept constant). As a result, there may be in fact slight variations in focal length as the camera was rotated.

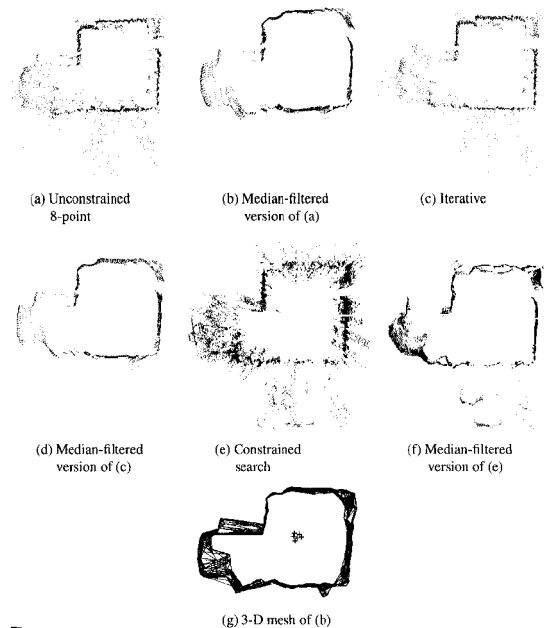


Figure 14. Extracted 3-D points and mesh of laboratory scene. The camera locations are indicated by +’s in (g).

- The camera may not be rotating exactly about its optical center, since the adjustment of the X-Y position stage is done manually and there may be human error in judging the absence of motion parallax.
- The camera may not be rotating about a unique axis all the way around (assumed to be vertical) due to some play or unevenness of the tripod.
- There were digitization problems. The images digitized from tape (i.e., while the camcorder is playing the tape) contain scan lines that are occasionally horizontally shifted; this is probably caused by the

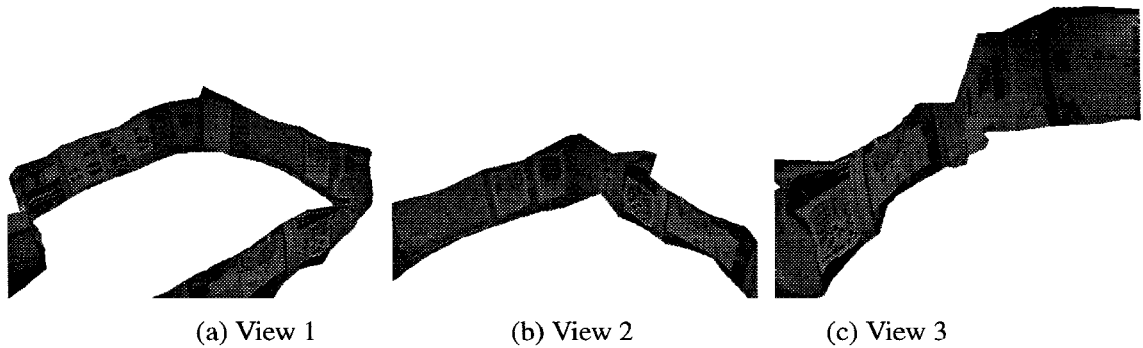


Figure 15. Three texture-mapped views of the modeled laboratory scene of Fig. 14(g).

degraded blanking signal not properly detected by the framegrabber. However, compositing many images averages out most of these artifacts.

- The extracted camera intrinsic parameters may not be very precise.

As a result of the problems encountered, the resulting composited panorama may not be physically correct. This especially causes problems with constrained search given the estimated epipolar geometry (through the essential matrix). We actually widened the search a little by allowing search as much as a couple of pixels away from the epipolar line. The results look only slightly better, however; while there is a greater chance of matching the correct locations, there is also a greater chance of confusion. This relaxed mode of search further increases the computational demand and has the effect of loosening the constraints, thus making this approach less attractive.

9. Discussion and Conclusions

We have shown that omnidirectional depth data (whose denseness depends on the amount of local texture) can be extracted using a set of simple techniques: camera calibration, image compositing, feature tracking, the 8-point algorithm, and constrained search using the recovered epipolar geometry. The advantage of our work is that we are able to extract depth data within a wide field of view simultaneously, which removes many of the traditional problems associated with recovering camera pose and narrow-baseline stereo. Despite the practical problems caused by using unsophisticated equipment which result in slightly incorrect panoramas, we are still able to extract reasonable 3-D data. Thus far, the best real data results come from using

unconstrained tracking and the 8-point algorithm (both direct and iterative structure from motion). Results also indicate that the application of 3-D median filtering improves both the accuracy and appearance of stereo-computed 3-D point distribution.

In terms of the differences between the three reconstruction methods, reconstruction methods 1 (8-point and direct 3-D calculation) and 2 (iterative structure from motion) yield virtually the same results, which suggests that the 8-point algorithm applied to panoramic images gives near optimal camera motion estimates. This is consistent with the intuition that widening the field of view with the attendant increase in image resolution results in more accurate estimation of egomotion; this was verified experimentally by Tian et al. (1996). One can then deduce that the iterative technique is usually not necessary. In the case of reconstruction method 3, where constrained search using the epipolar constraint is performed, denser data are obtained at the expense of much higher computation. In addition, the minimum and maximum depths have to be specified *a priori*. Based on real data results, the accuracy obtained using reconstruction method 3 is more sensitive to how physically correct the panoramas are composited. The compositing error can be attributed to the error in estimating the camera intrinsic parameters, namely the focal length and radial distortion factor (Kang and Weiss, 1996).

To expedite the panoramic image production in critical applications that require close to real-time modeling, special camera equipment may be called for. One such possible specialized equipment is Ahuja's camera system (as reported in Freedman, 1995; Krishnan and Ahuja, 1996), in which the lens can be rotated relative to the imaging plane. However, we are currently putting our emphasis on the use of commercially available equipment such as a cheap camcorder.

Even if all the practical problems associated with imperfect data acquisition were solved, we still have the fundamental problem of stereo—that of the inability to match and extract 3-D data in textureless regions. In scenes that involve mostly textureless components such as bare walls and objects, special pattern projectors may need to be used in conjunction with the camera (Kang et al., 1995).

Currently, the omnidirectional data, while obtained through a 360° view, has limited vertical view. We plan to extend this work by merging multiple omnidirectional data obtained at both different heights and at different locations. We will also look into the possibility of extracting panoramas of larger height extents by incorporating *tilted* (i.e., rotated about a horizontal axis) camera views. This would enable scene reconstruction of a building floor involving multiple rooms with good vertical view. We are currently characterizing the effects of misestimated intrinsic camera parameters (focal length, aspect ratio, and the radial distortion factor) on the accuracy of the recovered 3-D data.

In summary, our set of methods for reconstructing 3-D scene points within a wide field of view has been shown to be quite robust and accurate. Wide-angle reconstruction of 3-D scenes is conventionally achieved by merging multiple range images; our methods have been demonstrated to be a very attractive alternative in wide-angle 3-D scene model recovery. In addition, these methods do not require specialized camera equipment, thus making commercialization of this technology easier and more direct. We strongly feel that this development is a significant one toward attaining the goal of creating photorealistic 3-D scenes with minimum human intervention.

Appendix

A.1. Optimal Point Intersection

In order to find the point closest to all of the rays whose line equations are of the form $\mathbf{r} = \mathbf{t}_k + \lambda_k \hat{\mathbf{v}}_k$, we minimize the expression

$$\mathcal{E} = \sum_k \|\mathbf{p} - (\mathbf{t}_k + \lambda_k \hat{\mathbf{v}}_k)\|^2 \quad (\text{A1})$$

where \mathbf{p} is the optimal point of intersection to be determined. Taking the partials of \mathcal{E} with respect to λ_k and \mathbf{p} and equating them to zero, we have

$$\frac{\partial \mathcal{E}}{\partial \lambda_k} = 2\hat{\mathbf{v}}_k^T (\mathbf{t}_k + \lambda_k \hat{\mathbf{v}}_k - \mathbf{p}) = 0 \quad (\text{A2})$$

$$\frac{\partial \mathcal{E}}{\partial \mathbf{p}} = -2 \sum_k (\mathbf{t}_k + \lambda_k \hat{\mathbf{v}}_k - \mathbf{p}) = 0. \quad (\text{A3})$$

Solving for λ_k in (A2), noting that $\hat{\mathbf{v}}_k^T \hat{\mathbf{v}}_k = 1$, and substituting λ_k in (A3) yields

$$\sum_k (\mathbf{t}_k - \hat{\mathbf{v}}_k (\hat{\mathbf{v}}_k^T \mathbf{t}_k) - \mathbf{p} + \hat{\mathbf{v}}_k (\hat{\mathbf{v}}_k^T \mathbf{p})) = 0,$$

from which

$$\begin{aligned} \mathbf{p} &= \left[\sum_k \mathbf{A}_k \right]^{-1} \left[\sum_k \mathbf{A}_k \mathbf{t}_k \right] \\ &= \left[\sum_k \mathbf{A}_k \right]^{-1} \left[\sum_k \mathbf{p}_k^* \right], \end{aligned} \quad (\text{A4})$$

where

$$\mathbf{A}_k = \mathbf{I} - \hat{\mathbf{v}}_k \hat{\mathbf{v}}_k^T$$

is the perpendicular projection operator for ray $\hat{\mathbf{v}}_k$, and

$$\mathbf{p}_k^* = \mathbf{t}_k - \hat{\mathbf{v}}_k (\hat{\mathbf{v}}_k^T \mathbf{t}_k) = \mathbf{A}_k \mathbf{t}_k$$

is the point along the viewing ray $\mathbf{r} = \mathbf{t}_k + \lambda_k \hat{\mathbf{v}}_k$ closest to the origin.

Thus, the optimal intersection point for a bundle of rays can be computed as a weighted sum of adjusted camera centers (indicated by \mathbf{t}_k 's), where the weighting is in the direction perpendicular to the viewing ray.

A more “optimal” estimate can be found by minimizing the formula

$$\mathcal{E} = \sum_k \lambda_k^{-2} \|\mathbf{p} - (\mathbf{t}_k + \lambda_k \hat{\mathbf{v}}_k)\|^2 \quad (\text{A5})$$

with respect to \mathbf{p} and λ_k 's. Here, by weighting each squared perpendicular distance by λ_k^{-2} , we are down-weighting points further away from the camera. The justification for this formula is that the uncertainty in $\hat{\mathbf{v}}_k$ direction defines a *conical* region of uncertainty in space centered at the camera, i.e., the uncertainty in point location (and hence the inverse weight) grows linearly with λ_k . However, implementing this minimization requires an iterative non-linear solver.

A.2. Elemental Transform Derivatives

The derivative of the projection function (11) with respect to its 3-D arguments and internal parameters is

straightforward:

$$\frac{\partial \mathcal{P}(\mathbf{x})}{\partial \mathbf{x}} = \frac{1}{D} \begin{pmatrix} y^2 + z^2 & -xy & -xz \\ -xy & x^2 + z^2 & -yz \\ -xz & -yz & x^2 + y^2 \end{pmatrix},$$

where

$$D = (x^2 + y^2 + z^2)^{\frac{3}{2}}$$

The derivatives of an elemental rigid transformation (9)

$$\mathbf{x}' = \mathbf{R}\mathbf{x} + \mathbf{t}$$

are

$$\frac{\partial \mathbf{x}'}{\partial \mathbf{x}} = \mathbf{R}, \quad \frac{\partial \mathbf{x}'}{\partial \mathbf{t}} = \mathbf{I},$$

and

$$\frac{\partial \mathbf{x}'}{\partial \mathbf{q}} = -\mathbf{RC}(\mathbf{x})\mathbf{G}(\mathbf{q}),$$

where

$$\mathbf{C}(\mathbf{x}) = \begin{pmatrix} 0 & -z & y \\ z & 0 & -x \\ -y & x & 0 \end{pmatrix}$$

and

$$\mathbf{G}(\mathbf{q}) = 2 \begin{pmatrix} -q_0 & w & q_2 & -q_1 \\ -q_1 & -q_2 & w & q_0 \\ -q_2 & q_1 & -q_0 & w \end{pmatrix}$$

(see (Shabana, 1989)). The derivatives of a screen coordinate with respect to any motion or structure parameter can be computed by applying the chain rule and the above set of equations.

Acknowledgments

We would like to thank Andrew Johnson for the use of his 3-D modeling and rendering program and Richard Weiss for helpful discussions.

Notes

1. For a pair of images taken at two different locations, the epipoles are the location on the image planes which are the intersection between these image planes and the line joining the two camera optical centers. An excellent description of the stereo vision is given in Faugeras (1993).

2. Note that in general, a “worse” track in this sense need not necessarily translate to a worse 3-D estimate. A high match error may be due to apparent object distortion at different viewpoints.

References

- Ayache, N. 1991. *Artificial Vision for Mobile Robots: Stereo Vision and Multisensory Perception*. MIT Press: Cambridge, Massachusetts.
- Azarbayejani, A. and Pentland, A.P. 1995. Recursive estimation of motion, structure, and focal length. *IEEE Transactions on Pattern Analysis and Machine Intelligence*, 17(6):562–575.
- Barnard, S.T. and Fischler, M.A. 1982. Computational stereo. *Computing Surveys*, 14(4):553–572.
- Bolles, R.C., Baker, H.H., and Marimont, D.H. 1987. Epipolar-plane image analysis: An approach to determining structure from motion. *International Journal of Computer Vision*, 1:7–55.
- Deriche, R., Zhang, Z., Luong, Q.-T., and Faugeras, O. 1994. Robust recovery of the epipolar geometry for an uncalibrated stereo rig. In *Third European Conference on Computer Vision (ECCV'94)*, Springer-Verlag: Stockholm, Sweden, pp. 567–576.
- Dhond, U.R. and Aggarwal, J.K. 1989. Structure from stereo—A review. *IEEE Transactions on Systems, Man, and Cybernetics*, 19(6):1489–1510.
- Faugeras, O.D. 1992. What can be seen in three dimensions with an uncalibrated stereo rig? In *Second European Conference on Computer Vision (ECCV'92)*, Springer-Verlag: Santa Margherita Liguere, Italy, pp. 563–578.
- Faugeras, O. 1993. *Three-Dimensional Computer Vision: A Geometric Viewpoint*. MIT Press: Cambridge, Massachusetts.
- Ferrie, F.P. and Levine, M.D. 1987. Integrating information from multiple views. In *IEEE Workshop on Computer Vision*, IEEE Computer Society, pp. 117–122.
- Freedman, D.H. 1995. A camera for near, far, and wide. *Discover*, 16(48):48.
- Hartley, R. 1995. In defence of the 8-point algorithm. In *Fifth International Conference on Computer Vision (ICCV'95)*, IEEE Computer Society Press, Cambridge, Massachusetts, pp. 1064–1070.
- Higuchi, K., Hebert, M., and Ikeuchi, K. 1993. Building 3-D models from unregistered range images. Technical Report CMU-CS-93-214, Carnegie Mellon University.
- Ishiguro, H., Yamamoto, M., and Tsuji, S. 1992. Omnidirectional stereo. *IEEE Transactions on Pattern Analysis and Machine Intelligence*, 14:257–262.
- Kang, S.B., Johnson, A., and Szeliski, R. 1995. Extraction of concise and realistic 3-D models from real data. Technical Report 95/7, Digital Equipment Corporation, Cambridge Research Lab.
- Kang, S.B., Webb, J., Zitnick, L., and Kanade, T. 1995. A multi-baseline stereo system with active illumination and real-time image acquisition. In *Fifth International Conference on Computer Vision (ICCV'95)*, Cambridge, Massachusetts, pp. 88–93.
- Kang, S.B. and Weiss, R. 1996. Characterization of errors in compositing panoramic images. Technical Report 96/2, Digital Equipment Corporation, Cambridge Research Lab.
- Kolb, C.E. 1994. *Rayshade User's Guide and Reference Manual*.
- Krishnan, A. and Ahuja, N. 1996. Panoramic image acquisition. In *IEEE Computer Society Conference on Computer Vision and Pattern Recognition (CVPR'96)*, San Francisco, California.

- Kuglin, C.D. and Hines, D.C. 1975. The phase correlation image alignment method. In *IEEE 1975 Conference on Cybernetics and Society*, New York, pp. 163–165.
- Longuet-Higgins, H.C. 1981. A computer algorithm for reconstructing a scene from two projections. *Nature*, 293:133–135.
- McMillan, L. and Bishop, G. 1995. Plenoptic modeling: An image-based rendering system. *Computer Graphics (SIGGRAPH'95)*, pp. 39–46.
- Murray, D.W. 1995. Recovering range using virtual multicamera stereo. *Computer Vision and Image Understanding*, 61(2):285–291.
- Okutomi, M. and Kanade, T. 1993. A multiple baseline stereo. *IEEE Transactions on Pattern Analysis and Machine Intelligence*, 15(4):353–363.
- Parvin, B. and Medioni, G. 1992. B-rep from unregistered multiple range images. In *IEEE Int'l Conference on Robotics and Automation*, IEEE Society, pp. 1602–1607.
- Press, W.H., Flannery, B.P., Teukolsky, S.A., and Vetterling, W.T. 1992. *Numerical Recipes in C: The Art of Scientific Computing*. Second edition, Cambridge University Press: Cambridge, England.
- Shabana, A.A. 1989. *Dynamics of Multibody Systems*. J. Wiley: New York.
- Shashua, A. 1994. Projective structure from uncalibrated images: Structure from motion and recognition. *IEEE Transactions on Pattern Analysis and Machine Intelligence*, 16(8):778–790.
- Shi, J. and Tomasi, C. 1994. Good features to track. In *IEEE Computer Society Conference on Computer Vision and Pattern Recognition (CVPR'94)*, IEEE Computer Society, Seattle, Washington, pp. 593–600.
- Shum, H.-Y., Ikeuchi, K., and Reddy, R. 1994. Principal component analysis with missing data and its application to object modeling. In *IEEE Computer Society Conference on Computer Vision and Pattern Recognition (CVPR'94)*, IEEE Computer Society, Seattle, Washington, pp. 560–565.
- Stein, G. 1995. Accurate internal camera calibration using rotation, with analysis of sources of error. In *Fifth International Conference on Computer Vision (ICCV'95)*, Cambridge, Massachusetts, pp. 230–236.
- Szeliski, R. 1994. Image mosaicing for tele-reality applications. Technical Report 94/2, Digital Equipment Corporation, Cambridge Research Lab.
- Szeliski, R. 1996. Video mosaics for virtual environments. *IEEE Computer Graphics and Applications*, pp. 22–30.
- Szeliski, R. and Coughlan, J. 1994. Hierarchical spline-based image registration. In *IEEE Computer Society Conference on Computer Vision and Pattern Recognition (CVPR'94)*, IEEE Computer Society, Seattle, Washington, pp. 194–201.
- Szeliski, R. and Kang, S.B. 1994. Recovering 3D shape and motion from image streams using nonlinear least squares. *Journal of Visual Communication and Image Representation*, 5(1):10–28.
- Szeliski, R., Kang, S.B., and Shum, H.-Y. 1995. A parallel feature tracker for extended image sequences. In *IEEE International Symposium on Computer Vision*, Coral Gables, Florida, pp. 241–246.
- Taylor, C.J., Debevec, P.E., and Malik, J. 1996. Reconstructing polyhedral models of architectural scenes from photographs. In *Fourth European Conference on Computer Vision (ECCV'96)*, Springer-Verlag: Cambridge, England, pp. 659–668.
- Tian, T.Y., Tomasi, C., and Heeger, D.J. 1996. Comparison of approaches to egomotion computation. In *IEEE Computer Society Conference on Computer Vision and Pattern Recognition*, San Francisco, CA, pp. 315–320.